NASA/TM—2005-213894

# Computational Study of Separating Flow in a Planar Subsonic Diffuser

Teryn DalBello
University of Toledo, Toledo, Ohio

Vance Dippold III and Nicholas J. Georgiadis
Glenn Research Center, Cleveland, Ohio

October 2005

The NASA STI Program Office . . . in Profile

Since its founding, NASA has been dedicated to the advancement of aeronautics and space science. The NASA Scientific and Technical Information (STI) Program Office plays a key part in helping NASA maintain this important role.

The NASA STI Program Office is operated by Langley Research Center, the Lead Center for NASA's scientific and technical information. The NASA STI Program Office provides access to the NASA STI Database, the largest collection of aeronautical and space science STI in the world. The Program Office is also NASA's institutional mechanism for disseminating the results of its research and development activities. These results are published by NASA in the NASA STI Report Series, which includes the following report types:

- TECHNICAL PUBLICATION. Reports of completed research or a major significant phase of research that present the results of NASA programs and include extensive data or theoretical analysis. Includes compilations of significant scientific and technical data and information deemed to be of continuing reference value. NASA's counterpart of peer-reviewed formal professional papers but has less stringent limitations on manuscript length and extent of graphic presentations.

- TECHNICAL MEMORANDUM. Scientific and technical findings that are preliminary or of specialized interest, e.g., quick release reports, working papers, and bibliographies that contain minimal annotation. Does not contain extensive analysis.

- CONTRACTOR REPORT. Scientific and technical findings by NASA-sponsored contractors and grantees.

- CONFERENCE PUBLICATION. Collected papers from scientific and technical conferences, symposia, seminars, or other meetings sponsored or cosponsored by NASA.

- SPECIAL PUBLICATION. Scientific, technical, or historical information from NASA programs, projects, and missions, often concerned with subjects having substantial public interest.

- TECHNICAL TRANSLATION. English-language translations of foreign scientific and technical material pertinent to NASA's mission.

Specialized services that complement the STI Program Office's diverse offerings include creating custom thesauri, building customized databases, organizing and publishing research results . . . even providing videos.

For more information about the NASA STI Program Office, see the following:

- Access the NASA STI Program Home Page at ***http://www.sti.nasa.gov***

- E-mail your question via the Internet to help@sti.nasa.gov

- Fax your question to the NASA Access Help Desk at 301–621–0134

- Telephone the NASA Access Help Desk at 301–621–0390

- Write to:
  NASA Access Help Desk
  NASA Center for AeroSpace Information
  7121 Standard Drive
  Hanover, MD 21076

NASA/TM—2005-213894

# Computational Study of Separating Flow in a Planar Subsonic Diffuser

Teryn DalBello
University of Toledo, Toledo, Ohio

Vance Dippold III and Nicholas J. Georgiadis
Glenn Research Center, Cleveland, Ohio

National Aeronautics and
Space Administration

Glenn Research Center

October 2005

Available from

NASA Center for Aerospace Information
7121 Standard Drive
Hanover, MD 21076

National Technical Information Service
5285 Port Royal Road
Springfield, VA 22100

Available electronically at http://gltrs.grc.nasa.gov

# Computational Study of Separating Flow in a Planar Subsonic Diffuser

Teryn DalBello
University of Toledo
Toledo, Ohio 43606

Vance Dippold III and Nicholas J. Georgiadis
National Aeronautics and Space Administration
Glenn Research Center
Cleveland, Ohio 44135

## Abstract

A computational study of the separated flow through a 2-D asymmetric subsonic diffuser has been performed. The Wind Computational Fluid Dynamics code is used to predict the separation and reattachment behavior for an incompressible diffuser flow. The diffuser inlet flow is a two-dimensional, turbulent, and fully-developed channel flow with a Reynolds number of 20,000 based on the centerline velocity and the channel height. Wind solutions computed with the Menter SST, Chien $k$-ε, Spalart-Allmaras and Explicit Algebraic Reynolds Stress turbulence models are compared with experimentally measured velocity profiles and skin friction along the upper and lower walls. In addition to the turbulence model study, the effects of grid resolution and use of wall functions were investigated. The grid studies varied the number of grid points across the diffuser and varied the initial wall spacing from $y^+ = 0.2$ to 60. The wall function study assessed the applicability of wall functions for analysis of separated flow. The SST and Explicit Algebraic Stress models provide the best agreement with experimental data, and it is recommended wall functions should only be used with a high level of caution.

## Introduction

Diffusers are integral parts of jet engines and many other devices that depend on fluid flow. Performance of a propulsion system as a whole is dependent on the efficiency of diffusers. Identification of separation within diffusers is important because separation increases drag and causes inflow distortion to engine fans and compressors. Diffuser flow computations are a particularly challenging task for Computation Fluid Dynamics (CFD) simulations due to adverse pressure gradients created by the decelerating flow, frequently resulting in separation. These separations are highly dependent on local turbulence level, viscous wall effects, and diffuser pressure ratio, which are functions of the velocity gradients and the physical geometry. Thus, turbulence modeling and geometry modeling become dominant factors that affect the ability of CFD to accurately predict flow through diffusers.

Obi et al. (ref. 1) performed extensive experimental investigations for an asymmetric planar diffuser using Laser Doppler Velocimetry to measure mean velocity and Reynolds stress components at axial stations throughout, and compared them to computations using a variety of turbulence models. Obi found that representing the anisotropy of Reynolds Stress (or Second Moment Closure) based $k$-ε turbulence models is crucial for capturing the turbulent flow separation in these types of problems.

Buice and Eaton (ref. 2) repeated the experimental work of Obi et al. (ref. 1) using a larger aspect ratio experimental apparatus, paying extra attention to the treatment of the endwall boundary layers. In addition, the straight tailpipe section of the diffuser was extended to facilitate an examination of the boundary layer downstream of reattachment.

The present work aims to reproduce Buice and Eaton's work (ref. 2) computationally, focusing on four aspects of CFD modeling and their effects on the diffuser flow computations. The first part focuses on the effect of the total number of grid points on the solution. The second part focuses on a $y^+$ variation and its effect on computed skin friction and velocity profiles with the SST turbulence model. The third part addresses a turbulence model study in which velocity profiles and skin friction are computed at nominal $y^+$ values of 0.2 with several available turbulence models in Wind. Finally, the fourth part focuses on the wall function feature in Wind, which allows the analyst to use fewer grid points when modeling the boundary layer, decreasing the computational time required to obtain solutions. The Buice and Eaton diffuser case allows the performance of Wind's wall function and turbulence model implementations to be assessed for a well-defined benchmark separated flow.

## Numerical Model

Calculations were obtained with Wind (ref. 3) version 5, a general purpose 3-D Computational Fluid Dynamics (CFD) code which solves the turbulent, time-dependent, Reynolds-Averaged Navier-Stokes (RANS) equations using a node-centered finite volume approach. Wind is the production solver of the NPARC Alliance, a joint code development group of NASA Glenn Research Center, USAF Arnold Engineering Development Center, and the Boeing Company. In addition to perfect gas capabilities, Wind can also solve the equations which govern equilibrium air, non-equilibrium air, and frozen gas chemistry. For this study, the solver was configured to run with the following specifications:

- 2-D flow
- local time stepping (steady-state)
- Second-order Roe upwind scheme with modification for stretched grids
- Spalart-Allmaras (ref. 4) (S-A), Menter Shear Stress Transport (ref. 5) (SST), Chien $k$-ε (ref. 6), and Rumsey-Gatski $k$-ε Explicit Algebraic Reynolds Stress (refs. 7 and 8) (EASM) turbulence models
- Perfect gas, air, $\gamma = 1.4$

The Spalart-Allmaras turbulence model has been shown to perform well for attached and separated wall bounded flows. A rotation and curvature correction (ref. 9) is available for the Spalart-Allmaras model to account for streamline rotation and curvature, especially in duct flows. The Chien $k$-ε model is a widely used variant of the standard $k$-ε model with near wall treatments allowing turbulence, $k$, and dissipation, ε, to be set to zero at no-slip walls, facilitating treatment within CFD frameworks. A variable $C_\mu$ correction (ref. 10) available with the Chien $k$-ε model is designed to improve performance in adverse pressure gradient flows. The SST model combines the $k$-ω formulation to treat inner regions of wall boundary layers with a transformed $k$-ε formulation to handle the outer, mixing regions of the flow. The $k$-ε based EASM has been recently installed in Wind to better predict flows with strong anistropy and is also being used as a foundation for future turbulence model development work. The EASM is derived from a simplified form of the Reynolds Stress transport equation, which eliminates the limitations of the Boussinesq approximation and enables the model to predict anistropy among the Reynolds normal stresses. However, due to the algebraic nature of the resulting turbulent stress expressions, EASM is not significantly more computationally expensive than linear two-equation models.

The S-A and SST solutions were started from scratch. The $k$-ε calculations were started from the SST solutions. Lastly, the EASM solution was started from a $k$-ε solution.

The diffuser flow boundary conditions are shown in table 1. The inflow conditions were specified using Wind's Arbitrary Inflow boundary condition. Total pressure and temperature were held constant at the inflow boundaries. The static pressure across the outflow boundary was specified to that measured in

TABLE 1.—DIFFUSER FLOW BOUNDARY CONDITIONS

| | |
|---|---|
| Inflow total pressure | 14.7 lb/in$^2$ |
| Inflow total temperature | 530° R |
| Inflow Mach number | 0.0588981 |
| Outflow static pressure | 14.65 lb/in$^2$ |
| Turbulence (% of freestream velocity) | 0.00014 |

the experiment (14.65 lb/in$^2$). The upstream channel was made sufficiently long to obtain fully developed turbulent channel flow at the inlet of the diffuser section.

The solutions were run with a CFL number of five. A typical solution took approximately 130,000 iterations to converge. The convergence criterion consisted of monitoring skin friction values and velocity profiles for changes with iteration, reduction of several orders of magnitude in the residual error, and conservation of mass within the diffuser.

## Wall Functions

The Wind code uses the White-Christoph law of the wall (ref. 11) in its wall function formulation. The law of the wall assumes that, for attached flow, the flow in the logarithmic portion of the boundary layer behaves according to:

$$u^+ \equiv \frac{U^*}{U} = f\left(y^+\right) \tag{1}$$

The non-dimensional characteristic wall coordinate, $y^+$, is defined by:

$$y^+ = \frac{y \cdot U^* \cdot \rho_w}{\mu_w} \tag{2}$$

where $y$ is the dimensional distance between the wall and the first grid point off the wall, $\mu$ is the absolute viscosity obtained from Sutherland's law, and $\rho$ is the density. The wall friction velocity, $U^*$, is defined as:

$$U^* = \sqrt{\frac{\tau_w}{\rho_w}} \tag{3}$$

where $\tau_w$ is the shear stress at the wall. The use of a wall function in a computational flow solver allows fewer points to be placed near the wall: whereas points are typically packed to $y^+ \sim 1$ for a wall integration grid, initial grid point spacing typically ranges from $y^+ = 15$ to $y^+ = 100$ near the wall in a wall function grid. The effect of the initial grid point spacing is investigated in this paper. Wall functions can enable substantial savings in computational costs: increasing the initial grid point spacing reduces the total number of grid points and increases the limiting time stepping which usually corresponds to the smallest computational cell.

## Computational Grids and Diffuser Geometry

### Diffuser Geometry

The computational domain models the experimental apparatus of Buice and Eaton (ref. 2) (see fig. 1). The diffuser apparatus can be divided into three sections: an inflow channel, the asymmetric diffuser, and

an outflow channel. Buice and Eaton used the channel height, $H = 0.591$ inches, as their reference length. The inflow channel section has a length of $110H$. The diffuser has a 10 degree expansion angle and is $21H$ in length. At the end of the expansion, the diffuser channel is $4.7H$ in height. The axial station corresponding to the beginning of the expansion section is set as $x/H = 0$.

## Baseline Grid

Two-dimensional, structured, computational grids were generated for all cases using Pointwise, Inc.'s Gridgen (ref. 12) software. Figure 2(a) shows a trace of the entire computational domain. Figure 2(b) shows detail of the diffuser section highlighting the baseline 341×81 grid details (initial wall spacing set to $y^+ = 0.2$).

Two types of grid dependence studies were completed to define the baseline grid. The first study examined the overall grid resolution in terms of the total number of points spread vertically across the domain. The wall spacing for each of these grids was held constant, and the grids have the same number of axial points, 341. The second grid dependence study investigated the grid resolution, or spacing, near the wall, termed the "$y^+$ study," with each grid having the same number of points vertically and axially across the domain.

In order to determine the overall grid resolution required to get a grid independent solution, a grid sensitivity study was conducted on three different grid levels; the coarse being at 341×41, medium at 341×81, and fine at 341×161. The grid point spacing in the transverse ($j$-direction) decreases as more points are placed transversely across the diffuser. At a particular location in the axial direction ($i$-direction), the grid fineness can be measured as the maximum grid point spacing in the transverse direction, normalized by the local height of the diffuser:

$$fineness_i = \frac{(y_{i,j} - y_{i,j-1})_{\max}}{y_{i,jmax} - y_{i,j\min}} \tag{4}$$

For the coarse grid, the value of $fineness_i$ ranges from 0.075 to 0.097. The grid fineness is $fineness_i = 0.032$ to 0.043 for the medium grid and $fineness_i = 0.013$ to 0.019 for the fine grid. The average $y^+$ value at the wall for this study was one, and results were computed with the SST turbulence model. The medium grid and fine grid solutions were essentially identical, so the medium grid was selected for the calculations in this paper. The specific results of the grid dependence study will be discussed in the results section.

The $y^+$ study examined grid spacing at the wall ranging from a $y^+$ of 0.2 to 15 for the 341×81 grid. Recall that $y^+$ is the non-dimensional characteristic wall coordinate defined in equation (2). When calculating $U^*$ in equation (3), the shear stress at the wall, $\tau_w$, is defined as:

$$\tau_w = \tfrac{1}{2} \cdot C_f \cdot \rho \cdot U_b^2 \tag{5}$$

where $C_f$ is the skin friction coefficient. In the fully-developed entrance channel flow ($x/H$~0), Buice and Eaton (ref. 2) found $C_f = 0.0061$. This $C_f$ value was used to determine initial wall spacing. The bulk velocity in the channel, $U_b$, defined by:

$$U_b = \tfrac{1}{H} \cdot \int_0^H U \cdot dy \Big|_{\text{inflow}} \tag{6}$$

where $U$ is the axial velocity as a function of the vertical position. By conservation of mass for this incompressible flow, this integral may be evaluated anywhere in the constant area duct to yield the same value of $U_b$. Again, the experimental data from Buice and Eaton (ref. 2) was assumed, in which

$U_b$ = 65.6 ft/s (20 m/s). As is the convention, a constant initial grid point spacing was used for the entire grid, insuring that the grid is sufficiently packed across the laminar sublayer at all points. Results for the $y^+$ study are discussed in more detail in the results section.

## Wall Function Grids

A total of six cases were run using wall functions on the Buice and Eaton diffuser. These cases were divided into two sets of three grids; in which each set included grids with a specified spacing between the wall and the first grid point adjacent to the wall, or "initial grid point spacing." With the wall function option turned on, Wind implements wall functions when this second grid point has a calculated $y^+$ value greater than 15 (ref. 13). For portions of the grid where the initial grid point spacing is less than $y^+ = 15$, wall integration is used even though the generally accepted higher-end values for use of wall integration is $y^+<5$.

This study examined wall function grids with initial grid point spacing at the wall of $y^+ = 15$, $y^+ = 30$, and $y^+ = 60$. These values of $y^+$ were chosen to assess Wind's wall function capabilities across several positions in the boundary layer logarithmic region. Similar to what was discussed earlier, values of $C_f$ and $U_b$ were assumed from the Buice and Eaton data to calculate the initial grid point spacing for a given $y^+$ value using equations (2), (3), (5), and (6). Table 2 lists the initial grid point spacing for $y^+$ values of 15, 30, and 60. It is important to note that because the initial grid point physical spacing was held constant through the entire grid, the $y^+$ value of the initial grid point varies with flow properties in equation (2). It will later be shown that the initial grid point spacing of $y^+ = 15$ allowed this study to observe what happens when Wind switches between wall functions and wall integration.

TABLE 2.—INITIAL GRID POINT SPACING AT WALL

| Nominal $y^+$ value | Initial Grid Point Spacing [ft] | Number of Points in $y$-direction |
|---|---|---|
| Baseline (0.2) | 8.72e-6 | 81 |
| 15 | 6.41e-4 | 63 |
| 30 | 1.28e-3 | 55 |
| 60 | 2.57e-3 | 45 |

As mentioned previously, two groups of three grids were used in the wall function portion of this study. The first group followed the method of creating wall function grids as recommended by the Wind User's Guide (ref. 14). For this method, the grid points between the wall and the grid point at a particular $y^+$ value are removed from the baseline grid. The Wind utility *cfsubset* was used to remove those points. The resulting number of points across the diffuser grid for each $y^+$ is given in table 2. This first set of grids shall be referred to as the "log layer packed" (LLP) wall function grids. Figures 3(a) and (b) show the baseline grid and a LLP wall function grid. The second group of grids was created by specifying the initial grid point spacing and redistributing the remaining points with the grid generator in a similar manner as typically done when creating a wall integration grid. These grids shall be referred to as the "log layer unpacked" (LLU) wall function grids, because the grid points are not packed tightly through the log layer in comparison to the baseline wall integration or LLP wall function grids. Figure 3(c) shows a LLU wall function grid and can be compared to the wall integration grid and LLP wall function grid in figures 3(a) and (b). This method of creating wall function grids is often used for simplicity, and it is important to assess the performance of this type of wall function grid. For consistency, the LLU wall function grids use the same number of grid points as with the LLP wall function grids. Details of the six cases run as part of the wall function study are given in table 3.

TABLE 3.—WALL FUNCTION STUDY CASE DETAILS. "LLP" = LOG LAYER PACKED; "LLU" = LOG LAYER UNPACKED

| Case | LLP, $y^+ = 15$ | LLP, $y^+ = 30$ | LLP, $y^+ = 60$ | LLU, $y^+ = 15$ | LLU, $y^+ = 30$ | LLU, $y^+ = 60$ |
|---|---|---|---|---|---|---|
| Nominal $y^+$ initial spacing | 15 | 30 | 60 | 15 | 30 | 60 |
| LLP wall function grid | X | X | X | | | |
| LLU wall function grid | | | | X | X | X |
| Grid points in $x$-direction | 371 | 371 | 371 | 371 | 371 | 371 |
| Grid points in $y$-direction | 63 | 55 | 45 | 63 | 55 | 45 |

# Post Processing

In order to provide a direct comparison with experimental data, results are presented by showing velocity profiles at several axial stations and skin friction values on the upper and lower walls. Axial and vertical positions are non-dimensionalized by $H$. The velocity profiles are normalized by $U_b$, defined in equation (6). The fully developed channel centerline velocity is $1.14U_b$. The skin friction coefficient $C_f$ is described as:

$$C_f = \frac{\tau_w}{\frac{1}{2} \cdot \rho \cdot U_b^2} \tag{7}$$

The shear stress $\tau_w$ is calculated as:

$$\tau_w \approx \mu \cdot \left( \frac{\partial U}{\partial y} \right)_{\text{wall}} \tag{8}$$

# Results

## Grid Dependency Study

A grid dependence study was conducted on three different grid levels; the coarse being at 341×41, medium at 341×81, and fine at 341×161. Each grid had an initial grid point spacing of $y^+ = 1.0$. Figure 4(a) shows the velocity profiles at axial stations across the diffusing section. Figures 4(b) and (c) show skin friction plots along the lower wall. The medium (341×81) and fine (341×161) grids show much closer agreement with the experimental data than the coarse grid (341×41). While the fine grid does show a small improvement over the medium grid, it took much longer to reach a converged solution (twice as many iterations with twice as many grid points). The computational cost of the fine grid far exceeded the minimal benefit of the improved solution. As a result, the medium grid (341×81) was used to obtain the results shown in the rest of this paper.

## $y^+$ Variations

A study of the effects of varying the $y^+$ values on the diffuser behavior is described next. Grids using reference $y^+$ values of 0.2, 1, 5, and 15 were analyzed. The solutions presented here were completed with the SST turbulence model. Figures 5(a) and (b) show the upper and lower wall skin friction plots, respectively, computed with the SST turbulence model. On the upper wall (fig. 5(a)), it can be seen that $y^+$ values of 0.2 and 1 give very similar results for $x/H<0$. Interestingly, all values of $y^+$ give similar

results for $x/H>0$ due to the fact that the lower velocity flow in this region means that one can afford a larger spacing at the wall because the actual values in the diffusing section are substantially smaller than the reference values. Therefore, physical wall spacing can be higher and still give similar results (because of the lower velocity flow). This is the case with the bottom wall (fig. 5(b)) as well. In the channel portion ($x/H<0$), differences in the skin friction values become apparent. Figure 5(c) shows the velocity profiles. It is clear that the variations in axial velocity are small, especially in stagnant and separated regions of the flow (towards the bottom wall).

For the following turbulence model study, an initial spacing of $y^+= 0.2$ was selected because of the variations noted in the constant area channel region of the flow and due to the usually tighter $y^+$ specification required by EASM formulations.

## Turbulence Model Variation

Figures 6(a) and (b) show the typical flow patterns in terms of axial velocity contours computed with the SST model. Figure 6(c) shows the extent of the separation region. Relatively thick boundary layers can be seen in conjunction with a higher-speed core indicative of fully-developed channel flow. The flow enters the diffuser and separates on the lower wall at about 3–4$H$ due to the adverse pressure gradient created by the reduction in flow velocity. A separation bubble forms along the lower wall, with subsequent turbulent reattachment downstream. The flow remains attached on the upper wall. Table 4 lists the separation and reattachment points ($x/H$) for the various turbulence models studied at a $y^+$ of 0.2.

TABLE 4.—LOWER WALL SEPARATION AND REATTACHMENT POINTS. "RC" = SPALART-ALLMARAS MODEL ROTATION AND CURVATURE CORRECTION (ref. 9); "VAR. $C_\mu$" = $k$-ε MODEL VARIABLE $C_\mu$ CORRECTION (ref. 10).

| Model Type | Separation [$x/H$] | Reattachment [$x/H$] |
|---|---|---|
| Experiment | 7.4 | 29.2 |
| SST | 2.52 | 29.69 |
| $k$-ε (var. $C_\mu$ ON) | 0.677 | 20.93 |
| $k$-ε (var. $C_\mu$ OFF) | 0.771 | 20.69 |
| S-A (RC OFF) | 4.34 | 31.39 |
| S-A (RC ON) | 3.84 | 32.62 |
| EASM | 6.40 | 28.08 |

Table 4 indicates that the $k$-ε model overpredicts the separated region by predicting separation to occur upstream of all other models, but as indicated in figure 7, it predicts a much smaller and thinner separation region compared to the other models. The SST model is next with separation beginning at 2.52$H$ downstream of diffuser inflow plane ($x/H = 0$), which is closer to the experimental value of 7.3$H$. Figure 7 shows that the separation region size is about the same for the EASM, S-A, and SST models. Of all the turbulence models examined, the EASM model gives the closest prediction of the experimental separation point with a value of 6.40$H$.

Figure 8(a) shows the velocity profiles downstream with all turbulence models. The $k$-ε model underpredicts the flow velocities in the core regions, and slightly overpredicts the flow velocities towards the lower wall. It predicts a more uniform spread of velocities in the vertical direction in the core region, agreeing with the results of Obi et al. (ref. 1). The EASM and SST models provide the best prediction overall to experimental data. Figures 8(b) and (c) show skin friction on both the lower and upper walls respectively. On the lower wall, the SST and S-A models agree very well with the experimental data. On the upper wall (fig. 8(c)), the SST again provides the best results. The S-A model underpredicts the data just downstream of the diffuser entrance, and the EASM model overpredicts the data in the same location. At $x/H>14$, the $k$-$\varepsilon$ model overpredicts the skin friction values and, at $x/H<14$, it underpredicts the skin fiction on both the upper and lower walls. In fact, the $k$-ε model predicts separation on the upper wall. The rotation and curvature correction for the S-A model had a negligible effect, which is expected because

there is not strong curvature in this geometry. The $k$-ε variable $C_\mu$ option had a slightly better effect on the upper wall. In the fully-developed region of the channel upstream of the diffuser, the SST model provides the highest and most accurate skin friction values and the $k$-$\varepsilon$ model the worst.

## Wall Function Analysis

As with the previous studies, the wall skin friction and axial velocity profiles are the primary measure of performance for the wall function analyses conducted with the SST turbulence model. Figures 9(a) and (b) show the skin friction along the lower and upper walls of the diffuser, respectively. All the solutions predict flow separation and reattachment on the lower wall and attached flow on the upper wall. Table 5 gives the points of separation and reattachment for each case. It may be observed that, as the initial grid point spacing is increased, the prediction of the separation and reattachment points vary substantially. Figures 10(a) and (b) show the $y^+$ values of the second grid point through the entire diffuser computational region. As expected, the $y^+$ values for each case are close to the nominal value of $y^+$ upstream of the diffuser. As the flow passes through the diffuser, the $y^+$ values drop significantly in the separated region. This is expected since, with a little manipulation of equations (2), (3), and (5),

$$y^+ \propto \sqrt{\tau_w} \propto \sqrt{C_f} \tag{9}$$

Therefore, for a constant value of $y$, $y^+$ decreases with skin friction.

TABLE 4.—LOWER WALL SEPARATION AND REATTACHMENT POINTS
"LLP" = LOG LAYER PACKED; "LLU" = LOG LAYER UNPACKED

| Case | Separation [$x/H$] | Reattachment [$x/H$] |
|---|---|---|
| Experiment | 7.4 | 29.2 |
| Baseline, $y^+ = 0.2$ (no wall function) | 2.52 | 29.69 |
| LLP, $y^+ = 15$ | 3.29 | 29.67 |
| LLP, $y^+ = 30$ | 5.90 | 29.01 |
| LLP, $y^+ = 60$ | 13.70 | 25.83 |
| LLU, $y^+ = 15$ | 1.91 | 29.90 |
| LLU, $y^+ = 30$ | 6.10 | 28.66 |
| LLU, $y^+ = 60$ | 13.37 | 25.07 |

Along the upper wall, only the LLP (log layer packed) $y^+$=15 wall function grid solution shows reasonable agreement with the experiment and baseline case. However, figures 9(a) and (b) show that this case suffers from rather low skin friction prediction upstream of the diffuser along both the upper and lower walls. This is significant because all the other analyses predict a similar level of skin friction in the region upstream of the diffuser. This appears to be a result of Wind not activating the wall function in this region. Figure 10(a) shows that the value of $y^+$ along the lower wall is actually less than 15 upstream of the diffuser. Because Wind only activates the wall functions when $y^+$>15, the wall functions are not activated and Wind is using full wall integration at this point in the flow.

For the $y^+ = 30$ and $y^+ = 60$ grid cases, discontinuities are observed in the plots of skin friction (figs. 9(a) and (b)) and in the plots of the $y^+$ values (figs. 10(a) and (b)). This again appears to be a result of Wind switching between using wall functions and wall integration (and even back to wall functions again) as the value of $y^+$ crosses the $y^+$=15 threshold for determining the use of wall functions. Again, wall functions are used when $y^+$>15 and wall integration is used when $y^+$<15. When the solution is post-processed, the deactivation and reactivation of the wall functions cause a small, but noticeable, discontinuity in the $y^+$ values and, more importantly, in the computed values of skin friction.

Axial velocity profiles through the diffuser are plotted for each case in figure 11. The $y^+$=15 wall function grid cases show very good agreement with the baseline case. As shown earlier, this is probably

because the second grid point $y^+$ values through the diffuser are much lower than 15, causing Wind to disable the wall functions and solve the flow using wall integration, which can handle separated flows. The $y^+ = 30$ wall function grid cases show reasonable agreement with the baseline case, deviating the most due to the delayed point of flow separation. The $y^+ = 60$ wall function grid cases show poor agreement with the baseline analysis through the entire flow.

The primary advantage of wall functions is the ability to trade solution fidelity for CPU time by reducing the number of grid points near the wall. Table 6 shows the total CPU time required by each analysis (run for the same number of iterations) and the CPU time savings over the baseline analysis. As one might expect, the CPU time scaled linearly with the number of grid points. In flows with conditions favorable for wall functions, CPU time can be reduced significantly by using wall functions without a large reduction in fidelity. In fact, convergence time may be even further reduced by the increased limiting time stepping associated with larger grid cell size near the wall, i.e., fewer iterations may be necessary. For flows with significant separation, wall functions are not recommended as they trade too much fidelity for CPU time savings, resulting in a poor prediction.

TABLE 6.—CPU TIMES OF WALL FUNCTION ANALYSES. "LLP"=LOG LAYER PACKED; "LLU"=LOG LAYER UNPACKED

| Case | CPU Time [hours] | CPU Time Savings | Grid Point Savings |
|---|---|---|---|
| Baseline, $y^+$=0.2 (no wall function) | 12.44 | 0.0% | 0.0% |
| LLP, $y^+$=15 | 9.62 | 22.7% | 22.2% |
| LLP, $y^+$=30 | 8.32 | 33.1% | 32.1% |
| LLP, $y^+$=60 | 6.79 | 45.4% | 44.4% |
| LLU, $y^+$=15 | 9.56 | 23.2% | 22.2% |
| LLU, $y^+$=30 | 8.26 | 33.6% | 32.1% |
| LLU, $y^+$=60 | 6.76 | 45.7% | 44.4% |

# Conclusions

Results from a computational study of the separated flow behavior through a 2-D asymmetric subsonic diffuser computed with the Wind CFD code have been presented. Using the SST turbulence model and an initial grid point spacing of $y^+ = 1$, a grid sensitivity study was performed by varying the number of grid points in the transverse direction across the diffuser. The study found that 81 grid points is sufficient for this class of flows. This corresponds to a grid fineness (see eq. (4)) of roughly 0.04. A sensitivity study of the initial grid point spacing ($y^+$ study) was also performed. The axial velocity profiles computed with $y^+$ values ranging from 0.2 to 15 were close. However, skin friction results indicated an initial grid point spacing of $y^+ = 0.2–1.0$ was necessary for best agreement with experimental skin friction data.

For the turbulence model study, the SST and EASM models provided the best predictions in comparison to experimental data in terms of skin friction and velocity profiles. The S-A, SST, and EASM models predicted the same size of separation region with small differences in the predicted location of separation. The $k$-ε model provided the least accurate results, underpredicting the separation point (just past the inflow plane to the diffuser), and size of the separation region on the lower wall. The $k$-ε model also predicted separation on the top wall, which did not occur in the experiment.

Wind's wall functions, while they have been shown to perform well for attached flow problems, have been found in this study to not be a good choice for flows with large amounts of separation. The log layer packed (LLP) wall function grids appeared to give better skin friction predictions in the attached channel flow when the wall functions were active. However, the wide range of skin friction and velocity predictions through the rest of the flow made the comparison inconclusive. Finally, it was determined that post-processing and interpreting results requires care when using wall functions.

# References


1. Obi, S., Aoki, K., and Masuda, S., "Experimental and Computational Study of Turbulent Separating Flow in an Asymmetric Plane Diffuser," Ninth Symposium on Turbulent Shear Flows, Kyoto, Japan, August 16–19, pp. 305–1 to 305–4, 1993.
2. Buice, C.U. & Eaton, J.K., "Experimental Investigation of Flow Through an Asymmetric Plane Diffuser," *Journal of Fluids Engineering*, vol. 122, pp. 433–435, 2000.
3. Nelson, C.C. and Power, G.D., "CHSSI Project CFD-7: The NPARC Alliance Flow Simulation System," AIAA Paper 2001–0594, 2001.
4. Spalart, P.R. & Allmaras, S.R., "A One-Equation Turbulence Model for Aerodynamic Flows," AIAA Paper 1992–0439, 1992.
5. Menter, F.R., "Two-Equation Eddy Viscosity Turbulence Models for Engineering Applications," *AIAA Journal*, vol. 32, no. 8, pp. 1598–1605, 1994.
6. Chien K.Y., "Predictions of Channel and Boundary layer Flows with a Low-Reynolds-Number Turbulence Model," *AIAA Journal*, vol. 20, no. 1, pp. 33–38, 1982.
7. Rumsey, C.L., Gatski, T.B., and Morrison, J.H., "Turbulence Model Predictions of Strongly Curved Flow in a U-Duct," *AIAA Journal*, vol. 38, no. 8, pp. 1394–1402, 2000.
8. Yoder, D.A., "Initial Evaluation of an Algebraic Reynolds Stress Model for Compressible Turbulent Shear Flows," AIAA Paper 2003–0548, 2003.
9. Mani, M., Ladd, J.A., and Bower, W.W., "Rotation and Curvature Correction Assessment for One-and Two-Equation Turbulence Models," *Journal of Aircraft*, vol. 41, no. 2, pp 268–273, 2004.
10. Rodi, W., and Scheuerer, G., "Scrutinizing the k-epsilon Turbulence Model Under Adverse Pressure Gradient Conditions," *Transactions of the ASME Journal of Fluids Engineering*, vol. 108, pp. 174–179, 1986.
11. White, F.M. and Christoph, G.H., "A Simple Theory for Two-Dimensional Compressible Turbulent Boundary Layer," *Journal of Basic Engineering*, vol. 94, pp. 636–642, 1972.
12. GRIDGEN Version 13, User Manual, Pointwise, Inc., Bedford, Texas, 1998.
13. Mani, M., "A Compressible Wall Function for Steady and Unsteady Flow Applications," 17th AIAA Applied Aerodynamics Conference, AIAA Paper 99–3216, 1999.
14. The Wind User's Guide Version 5, User Manual, The NPARC Alliance, Cleveland, OH. http://www.grc.nasa.gov/WWW/winddocs/index.html.

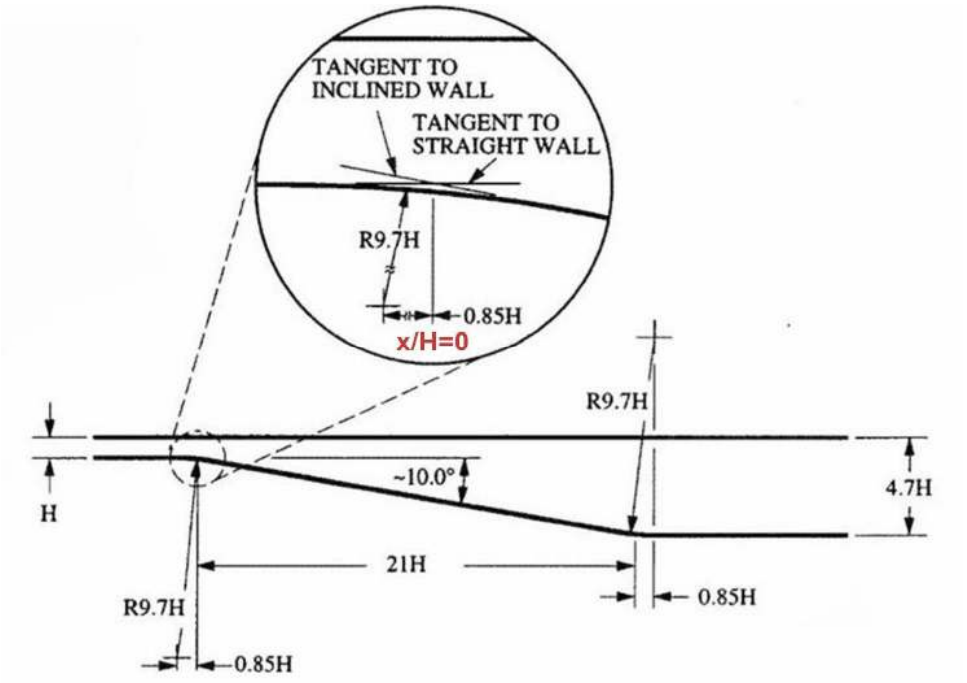


Figure 1.—Detailed schematic of diffuser layout (ref. 2).

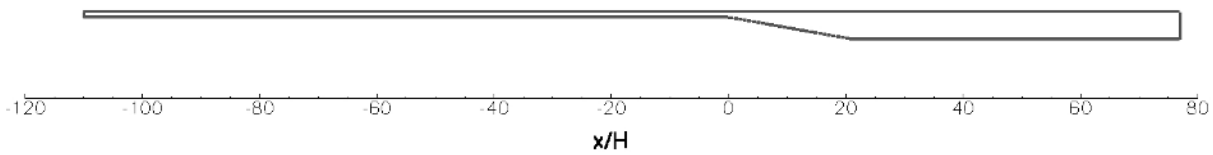


Figure 2(a).—Trace defining outer boundaries of computational domain.

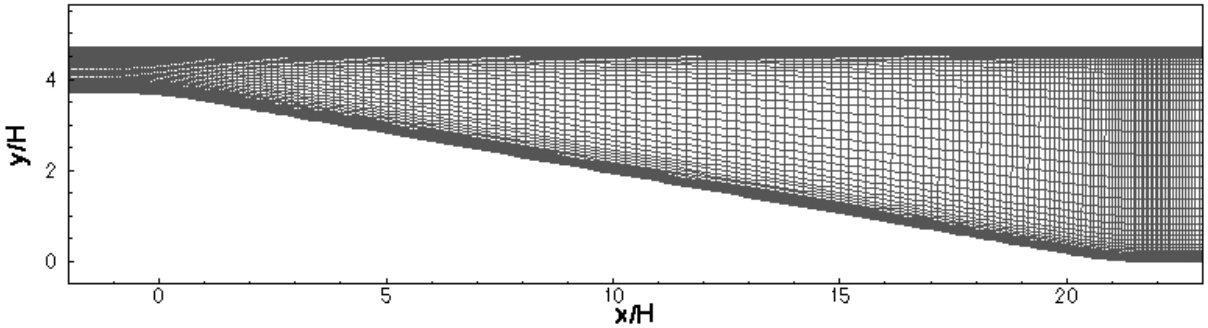


Figure 2(b).—Baseline 341×81 grid, diffuser section: $y^+ = 0.2$.

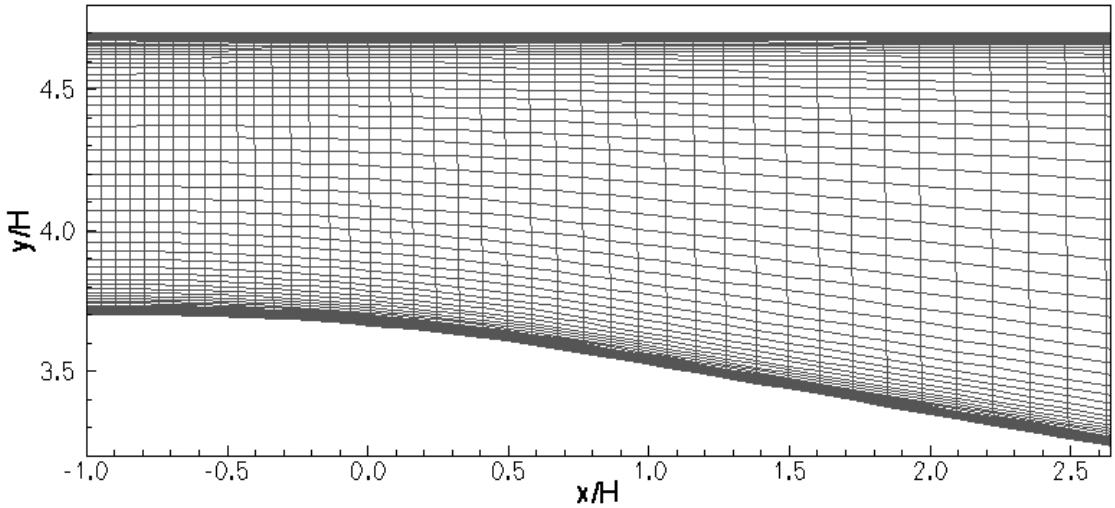


Figure 3(a).—Baseline wall integration grid: $y^+ = 0.2$.

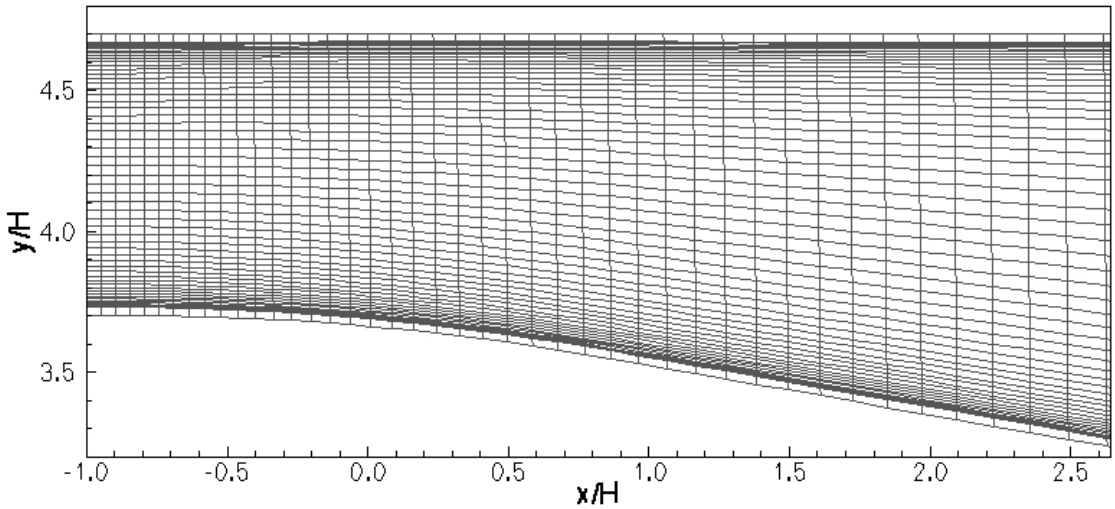


Figure 3(b).—Log layer packed (LLP) wall function grid: $y^+ = 30$.

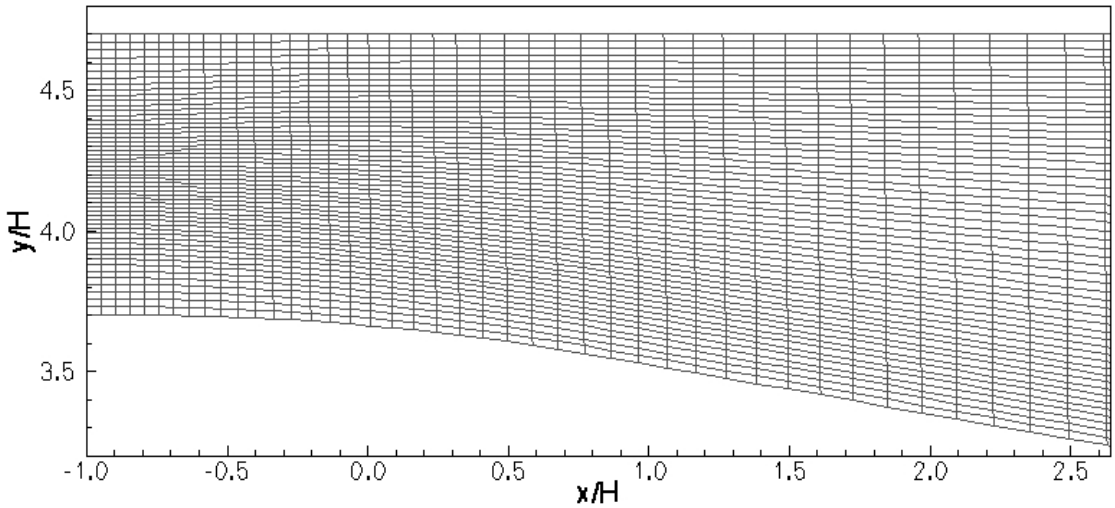


Figure 3(c).—Log layer unpacked (LLU) wall function grid: $y^+ = 30$.

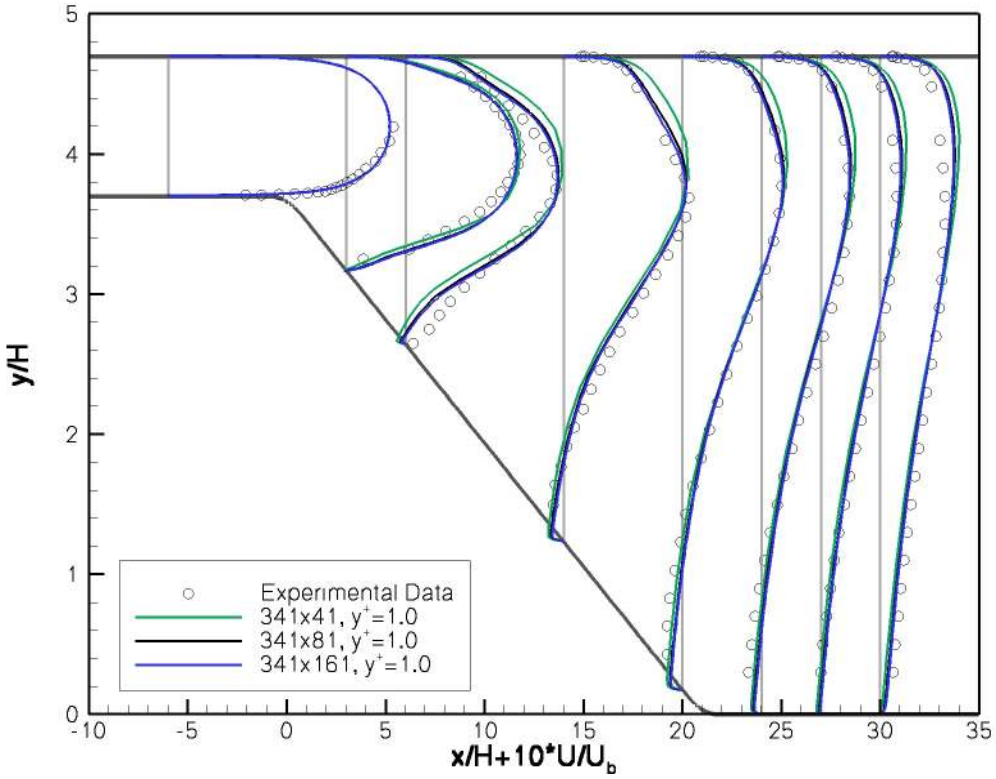


Figure 4(a).—Mean velocity profiles at different grid sizes using the SST model; $y^+ = 1$.

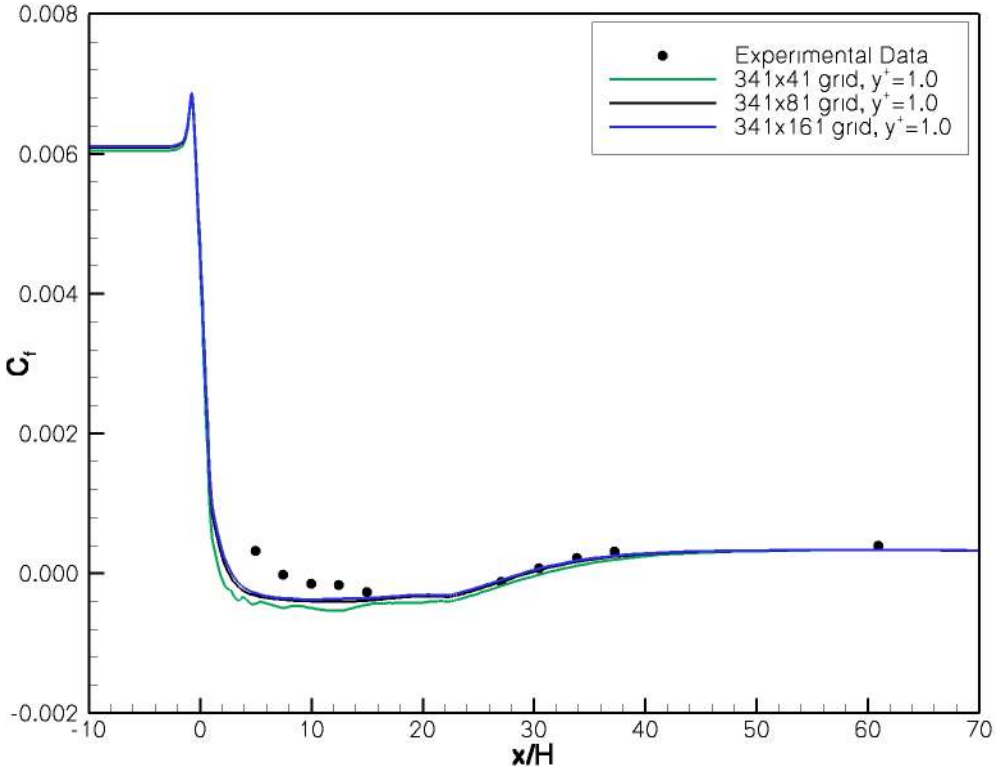


Figure 4(b).—Lower wall skin friction at different grid sizes using the SST model; $y^+ = 1$.

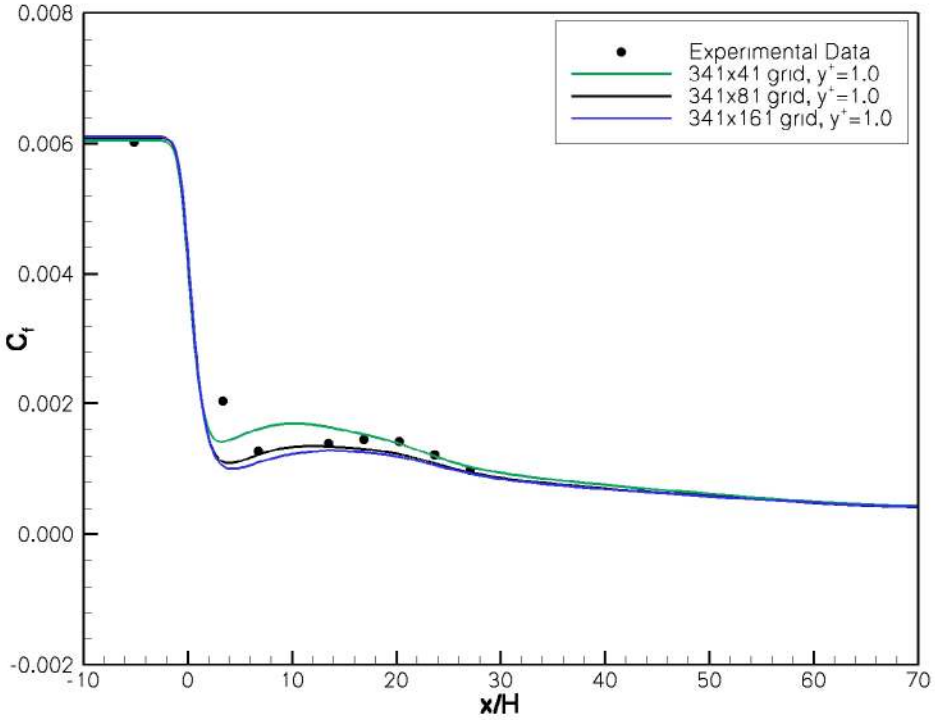


Figure 4(c).—Upper wall skin friction at different grid sizes using the SST model; $y^+ = 1$.

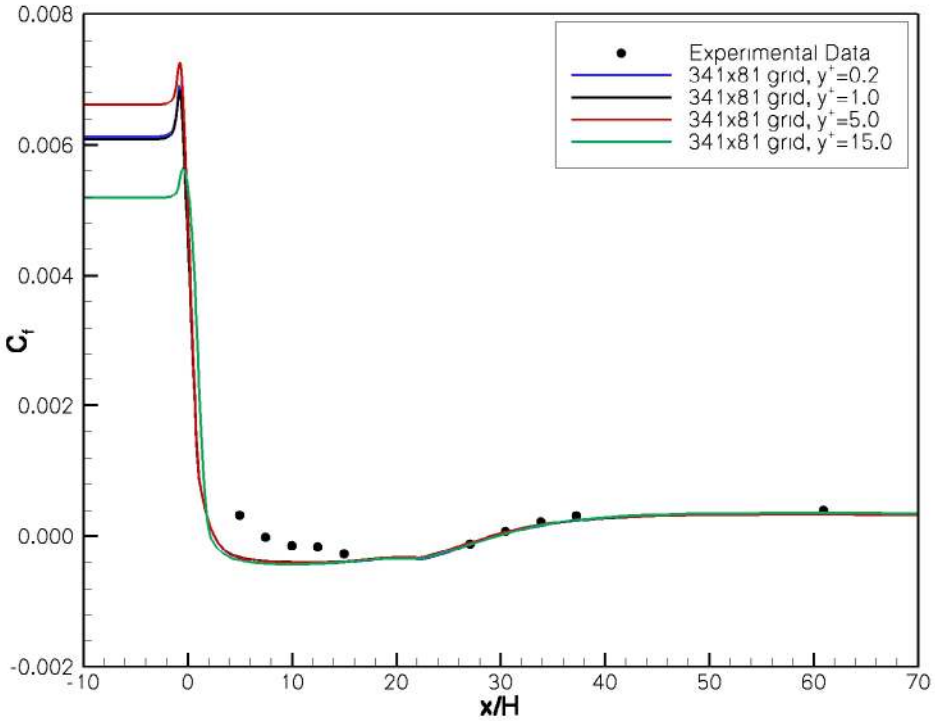


Figure 5(a).—Upper wall $C_f$ profiles using a range of $y^+$ values for 341×81 grids with SST model.

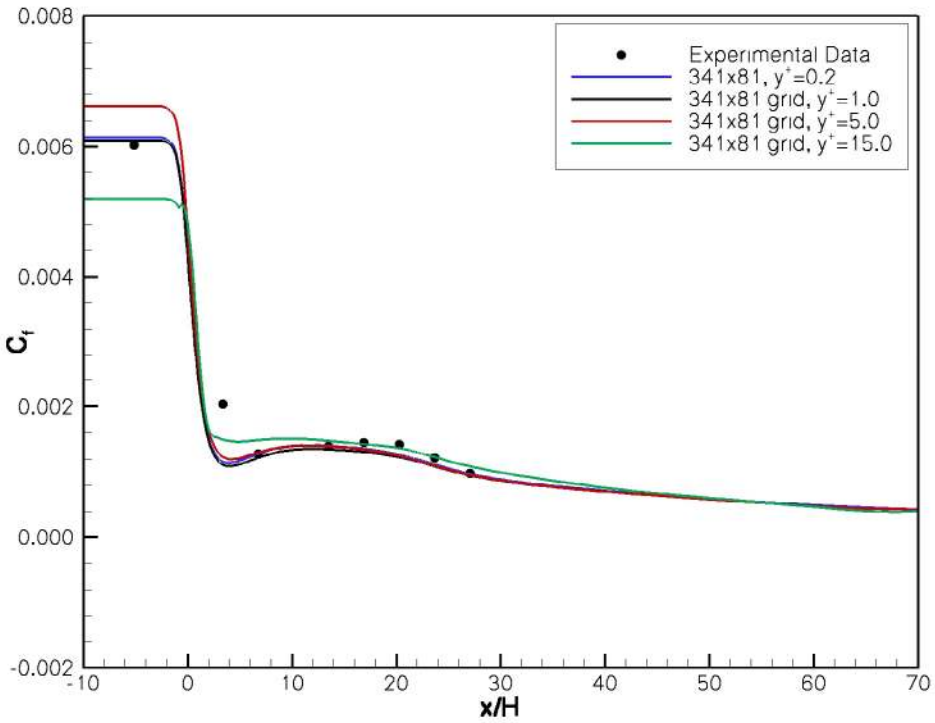


Figure 5(b).—Lower wall $C_f$ profiles using a range of $y^+$ values for 341×81 grids with SST model.

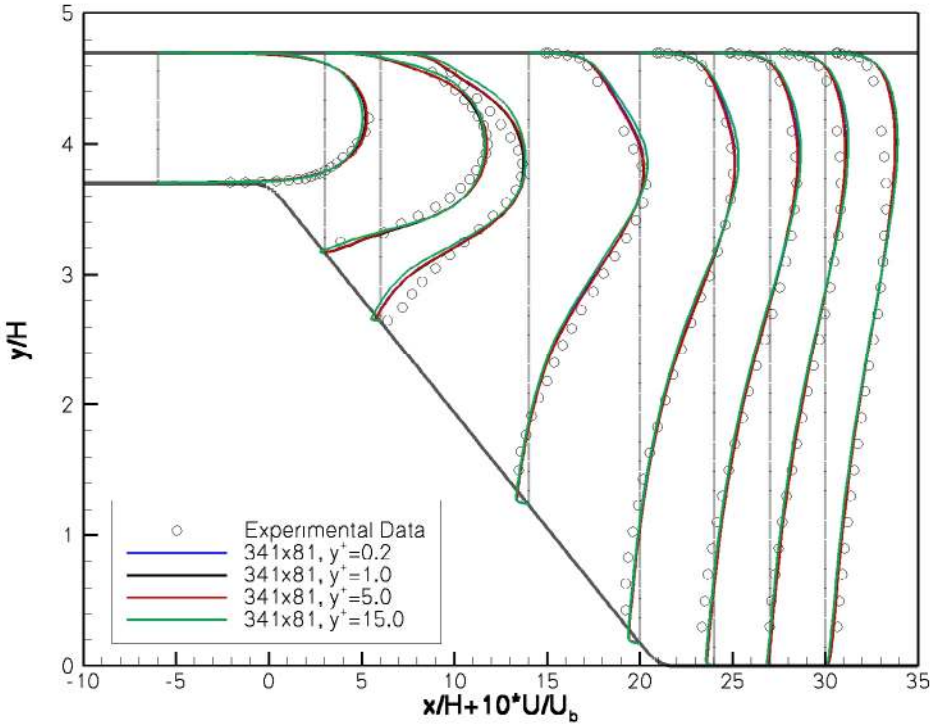


Figure 5(c).—Mean velocity profiles using a range of $y^+$ values for 341×81 grids with SST model.

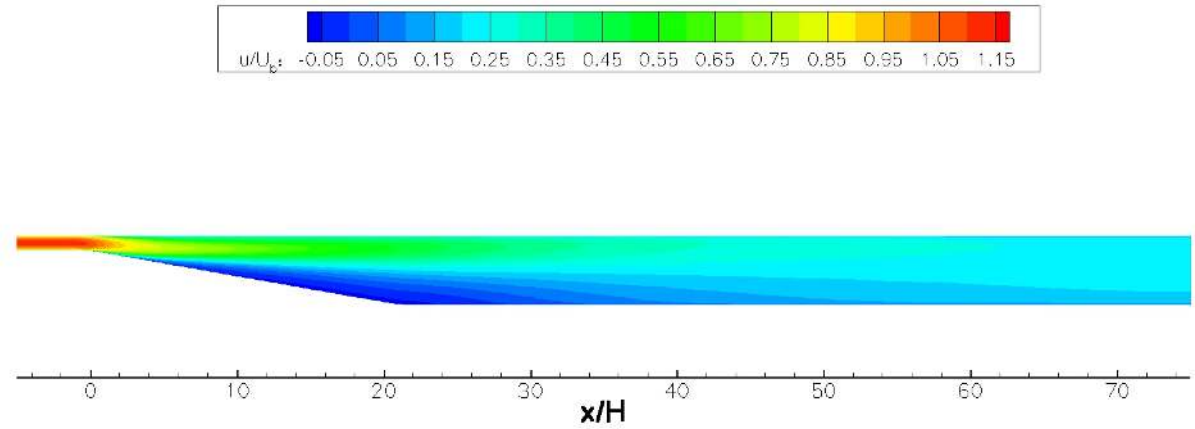


Figure 6(a).—Contours of axial velocity (normalized by $U_b$) plotted for entire diffuser SST model.

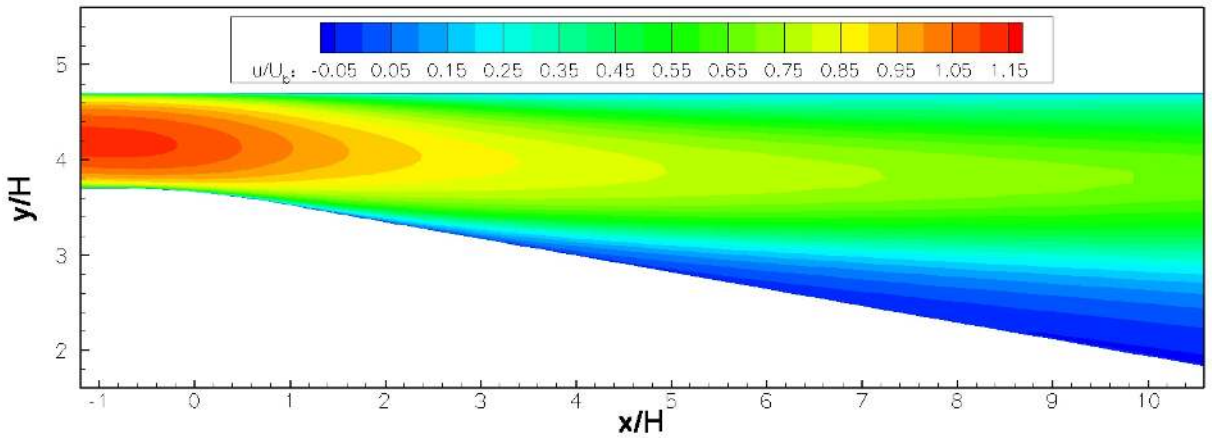


Figure 6(b).—Contours of axial velocity (normalized by $U_b$) at diffuser entrance SST model. (Detail view)

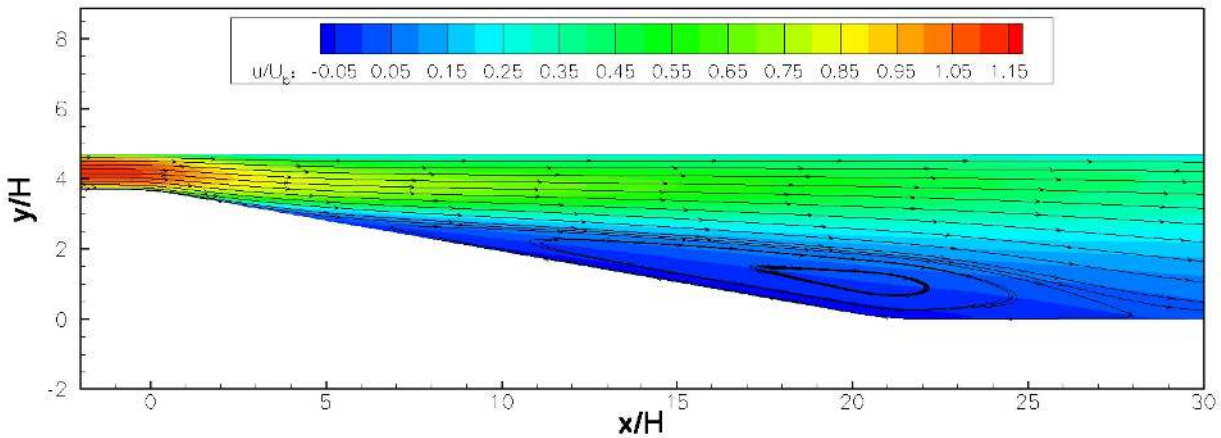


Figure 6(c).—Streamlines with contours of axial velocity (normalized by $U_b$) showing separated flow SST model.

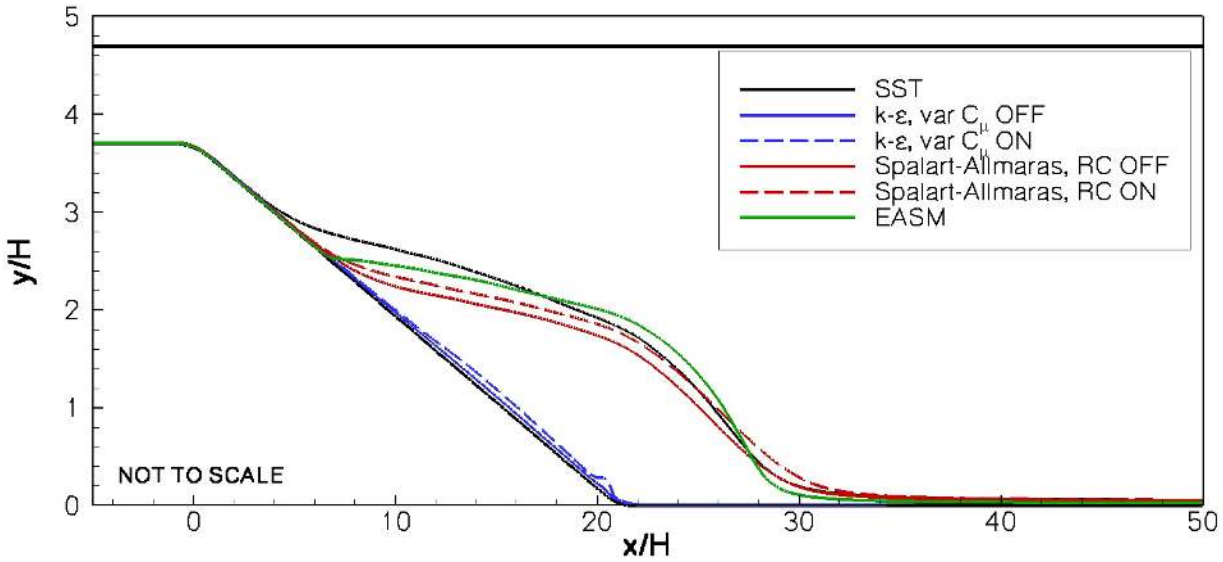


Figure 7.—Separation streamlines for all turbulence models on 341×81 grid with $y^+ = 1$. "RC" = Spalart-Allmaras model rotation and curvature correction (ref. 9); "var. $C_\mu$"=$k$-ε model variable $C_\mu$ correction (ref. 10).

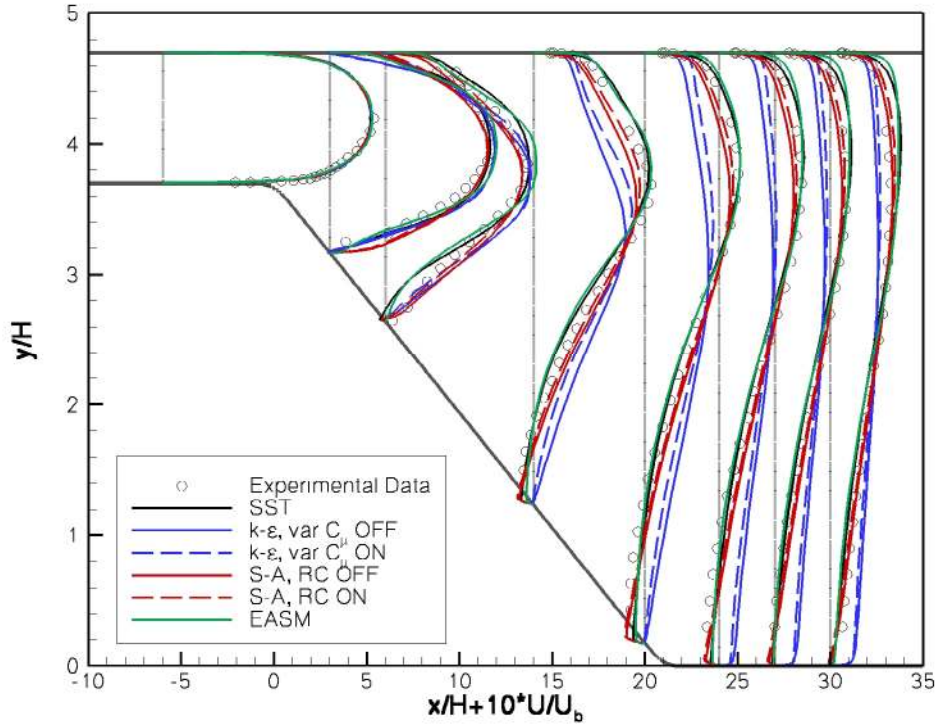


Figure 8(a).—Mean velocity profiles for all turbulence models on 341×81 grid with $y^+ = 1$. "RC" = Spalart-Allmaras model rotation and curvature correction (ref. 9); "var. $C_\mu$"=$k$-ε model variable $C_\mu$ correction (ref. 10).

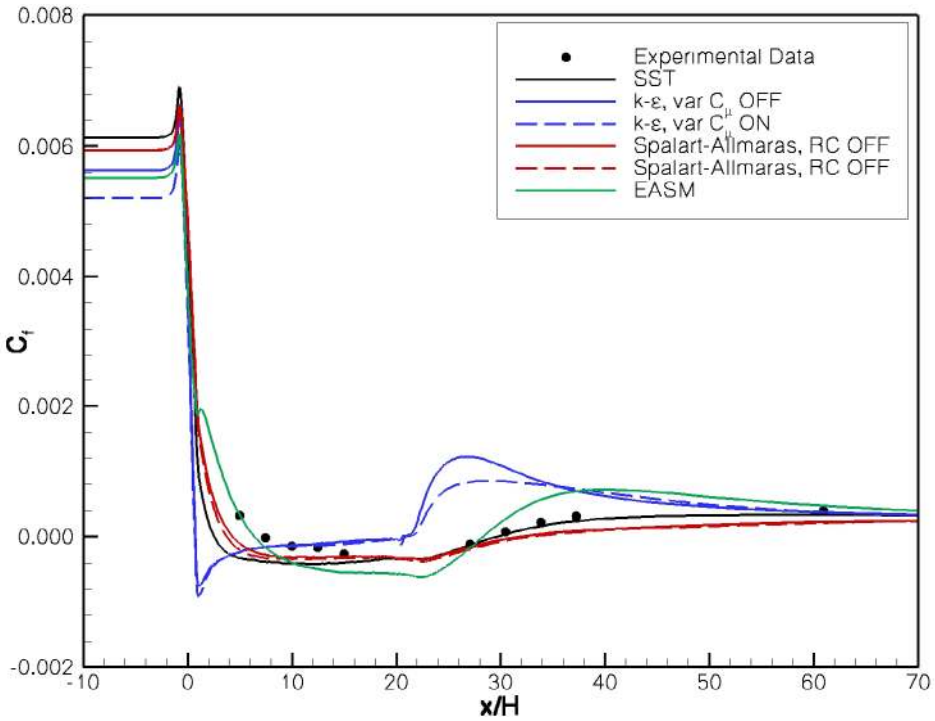


Figure 8(b).—Skin friction on lower wall for all turbulence models on 341×81 grid with $y^+ = 1$. "RC" = Spalart-Allmaras model rotation and curvature correction (ref. 9); "var. $C_\mu$" = $k$-ε model variable $C_\mu$ correction (ref. 10).

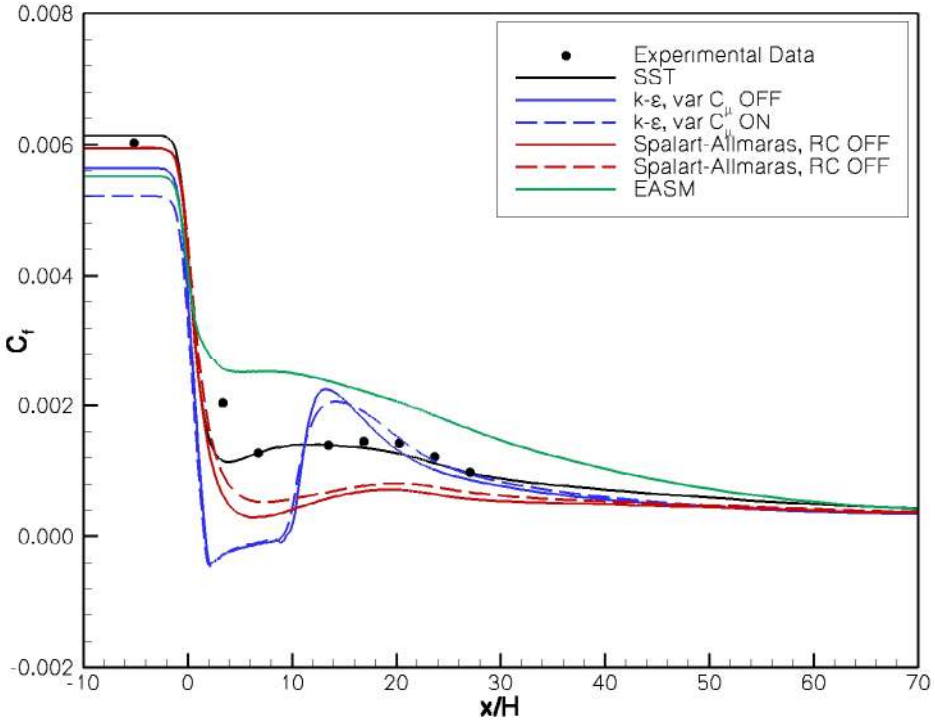


Figure 8(c).—Skin friction on upper wall for all turbulence models on 341×81 grid with $y^+ = 1$. "RC" = Spalart-Allmaras model rotation and curvature correction (ref. 9); "var. $C_\mu$"=$k$-ε model variable $C_\mu$ correction (ref. 10).

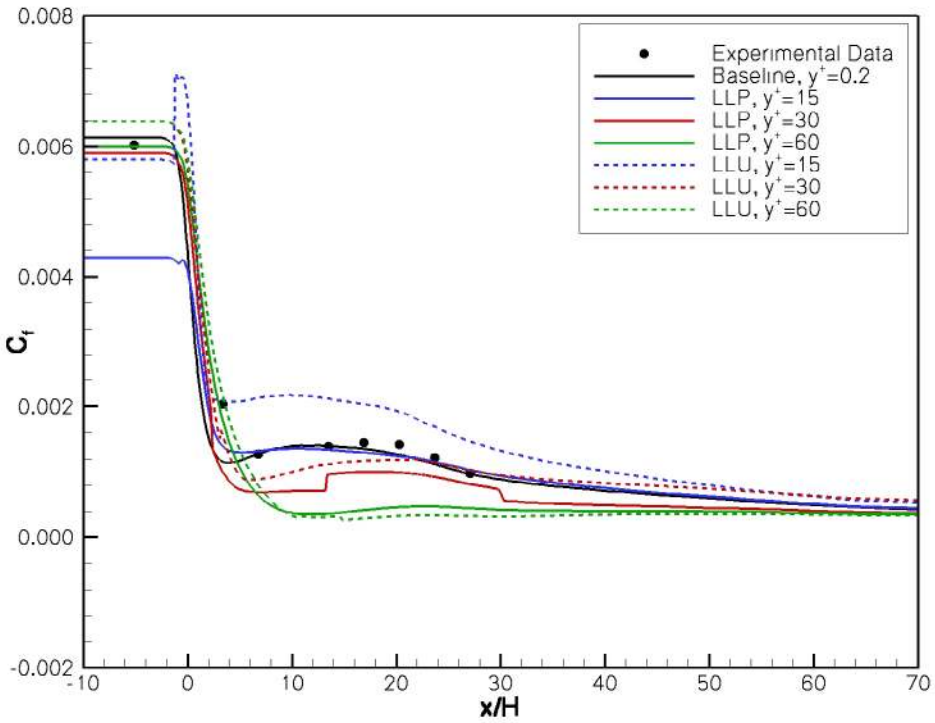


Figure 9(a).—Lower wall skin friction with SST model. "LLP" = Log Layer Packed; "LLU" = Log Layer Unpacked.

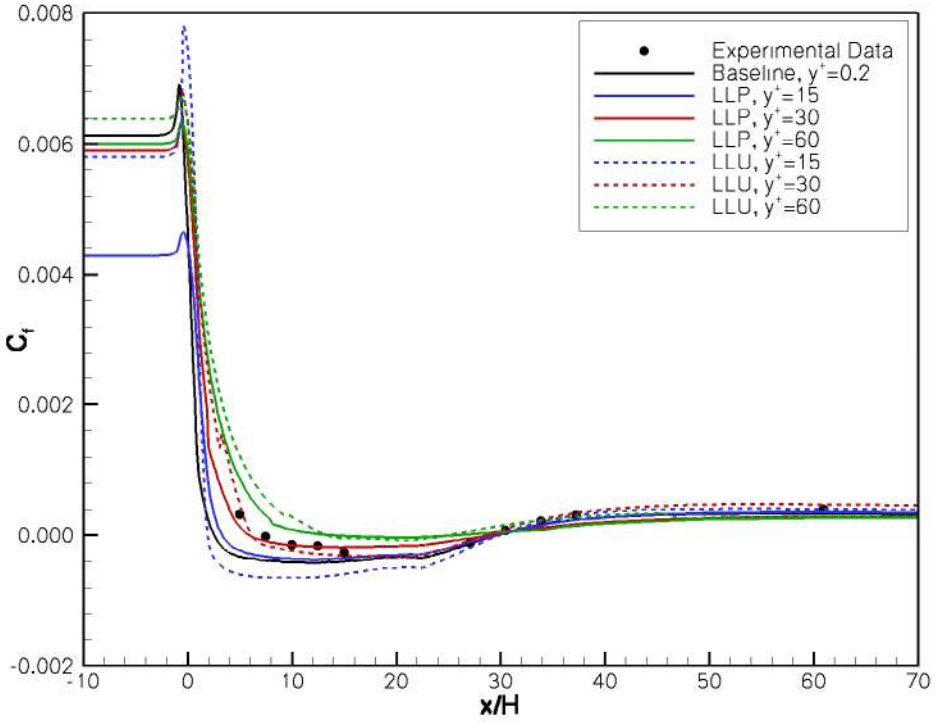


Figure 9(b).—Upper wall skin friction with SST model. "LLP" = Log Layer Packed; "LLU" = Log Layer Unpacked.

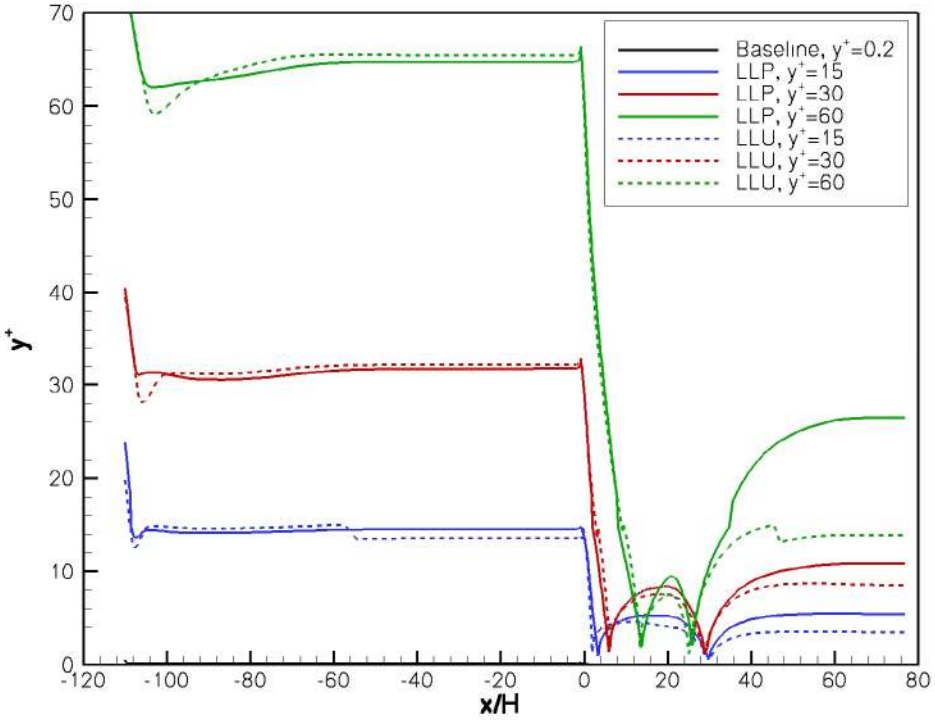


Figure 10(a).—Lower wall $y^+$ values with SST model. "LLP" = Log Layer Packed; "LLU" = Log Layer Unpacked.

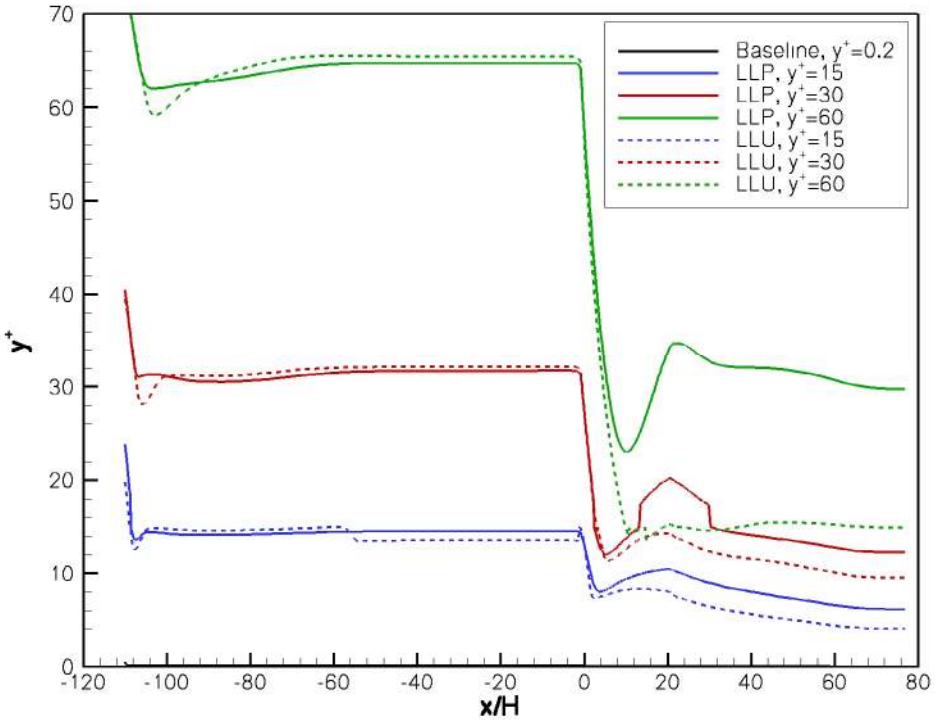


Figure 10(b).—Upper wall $y^+$ values with SST model. "LLP" = Log Layer Packed; "LLU" = Log Layer Unpacked.

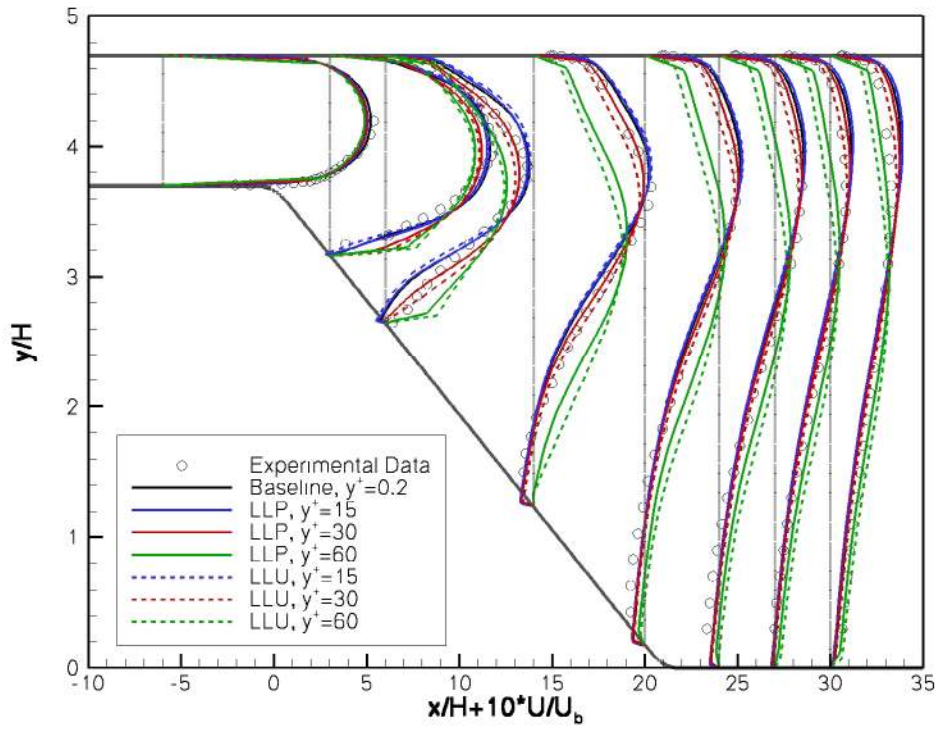


Figure 11.—Mean velocity profiles for wall function studies with SST model.

# REPORT DOCUMENTATION PAGE

*Form Approved*
*OMB No. 0704-0188*



| 1. AGENCY USE ONLY (*Leave blank*) | 2. REPORT DATE | 3. REPORT TYPE AND DATES COVERED |
|---|---|---|
| | October 2005 | Technical Memorandum |

**4. TITLE AND SUBTITLE**

Computational Study of Separating Flow in a Planar Subsonic Diffuser

**5. FUNDING NUMBERS**

WBS–22–781–30–70

**6. AUTHOR(S)**

Teryn DalBello, Vance Dippold III, and Nicholas J. Georgiadis

**7. PERFORMING ORGANIZATION NAME(S) AND ADDRESS(ES)**

National Aeronautics and Space Administration
John H. Glenn Research Center at Lewis Field
Cleveland, Ohio 44135–3191

**8. PERFORMING ORGANIZATION REPORT NUMBER**

E–15265

**9. SPONSORING/MONITORING AGENCY NAME(S) AND ADDRESS(ES)**

National Aeronautics and Space Administration
Washington, DC 20546–0001

**10. SPONSORING/MONITORING AGENCY REPORT NUMBER**

NASA TM—2005–213894

**11. SUPPLEMENTARY NOTES**

Teryn DalBello, University of Toledo, 2801 W. Bancroft Street, Toledo, Ohio 43606–3390; and Vance Dippold III and Nicholas J. Georgiadis, NASA Glenn Research Center. Responsible person, Vance Dippold III, organization code RTN, 216–433–8365.

**12a. DISTRIBUTION/AVAILABILITY STATEMENT**

Unclassified - Unlimited
Subject Category: 02

Available electronically at http://gltrs.grc.nasa.gov

This publication is available from the NASA Center for AeroSpace Information, 301–621–0390.

**12b. DISTRIBUTION CODE**

**13. ABSTRACT** ***(Maximum 200 words)***

A computational study of the separated flow through a 2-D asymmetric subsonic diffuser has been performed. The Wind Computational Fluid Dynamics code is used to predict the separation and reattachment behavior for an incompressible diffuser flow. The diffuser inlet flow is a two-dimensional, turbulent, and fully-developed channel flow with a Reynolds number of 20,000 based on the centerline velocity and the channel height. Wind solutions computed with the Menter SST, Chien $k$-ε, Spalart-Allmaras and Explicit Algebraic Reynolds Stress turbulence models are compared with experimentally measured velocity profiles and skin friction along the upper and lower walls. In addition to the turbulence model study, the effects of grid resolution and use of wall functions were investigated. The grid studies varied the number of grid points across the diffuser and varied the initial wall spacing from $y^+ = 0.2$ to 60. The wall function study assessed the applicability of wall functions for analysis of separated flow. The SST and Explicit Algebraic Stress models provide the best agreement with experimental data, and it is recommended wall functions should only be used with a high level of caution.

**14. SUBJECT TERMS**

Diffuser; Separated flow; CFD; Wind-US; Turbulence; Grid sensitivity

**15. NUMBER OF PAGES**

27

**16. PRICE CODE**

| 17. SECURITY CLASSIFICATION OF REPORT | 18. SECURITY CLASSIFICATION OF THIS PAGE | 19. SECURITY CLASSIFICATION OF ABSTRACT | 20. LIMITATION OF ABSTRACT |
|---|---|---|---|
| Unclassified | Unclassified | Unclassified | |